THE JOURNAL OF PHYSICAL CHEMISTRY C

Subscriber access provided by HEAL-Link (Hellenic Academic Libraries Link)

C: Physical Processes in Nanomaterials and Nanostructures

Electric Field Effect on Condensed-Phase Molecular Systems. VIII. Vibrational Stark Effect and Dipolar Inversion in Carbon Monoxide Crystal

Hani Kang, Josée Maurais, Youngwook Park, Patrick Ayotte, and Heon Kang

J. Phys. Chem. C, **Just Accepted Manuscript** • DOI: 10.1021/acs.jpcc.9b08902 • Publication Date (Web): 03 Dec 2019

is published by the American Chemical Society. 1155 Sixteenth Street N.W., Washington, DC 20036

Submitted to J. Phys. Chem. C (Revised Version)

Electric Field Effect on Condensed-Phase Molecular Systems. VIII. Vibrational Stark Effect and Dipolar Inversion in Carbon Monoxide Crystal

Hani Kang,[a] Josée Maurais,[b] Youngwook Park,[a] Patrick Ayotte,*[b] and Heon Kang*[a]

[a] *Department of Chemistry, Seoul National University, 1 Gwanak-ro, Seoul 08826, Republic of Korea*

[b] *Département de chimie, Université de Sherbrooke, 2500 Boulevard Université, Sherbrooke, Québec, Canada J1K 2R1*

Abstract

We applied a strong ($\leq 2.6 \times 10^8$ $V \cdot m^{-1}$) external electric field across a carbon monoxide crystal film at 10 K and studied its effect on the sample with reflection absorption infrared spectroscopy (RAIRS). The vibrational Stark effect (VSE) on the intramolecular CO stretching vibrations of the minor isotopologues ($^{13}C^{16}O$ and $^{12}C^{18}O$) reveal the spectral signature of isolated CO vibrations, decoupled from crystal phonons in the solid, as a function of the external electric field magnitude. These so-called molecular CO bands display a vibrational Stark effect (VSE) with a sensitivity factor of 0.69 ± 0.05 $cm^{-1}/(10^8\ V \cdot m^{-1})$ in crystalline CO. The VSE on the coupled CO stretching vibrations of the major isotopologue ($^{12}C^{16}O$) was measured for crystalline and amorphous solid CO films, and the results were analyzed with the help of a classical optics model of RAIRS for thin solid films. In addition to these spectral changes due to VSE, the external electric field facilitates the head-to-tail inversion of CO dipoles in the crystal lattice as a result of electrostatic interactions. This result is the first experimental demonstration of dipole inversion in a molecular crystal induced by a DC electric field. The dipole inversion occurs slowly and irreversibly in crystalline CO, reaching a yield of up to about 20% dipole inversion at an external field strength of 2.6×10^8 $V \cdot m^{-1}$ at 10 K. The observed yield of dipole inversion is interpreted in terms of a thermodynamic model that accounts for the electrostatic stabilization energy of dipoles and the configurational entropy of the CO crystal. The present study demonstrates that a polarized CO crystal with reduced residual entropy can be formed by applying a strong electric field at low temperature.

1. Introduction

Carbon monoxide and carbonyl functional groups are widely used as a chromophore in vibrational Stark effect (VSE) spectroscopy, which measures the vibrational frequency shift of molecules induced by electric fields.[1] The CO stretching band is readily detectable with infrared spectroscopy in a spectral region well separated from the absorption bands of many solvent molecules, and the VSE of CO provides a sensitive proxi for the local electric field strength in complex environments.[1-12] VSE studies have reported that CO molecules dissolved in amorphous solid films of 2-methyl tetrahydrofuran (THF)[3] or water[6] have a Stark sensitivity factor ($\Delta\mu$) of 0.6-0.7 $cm^{-1}/(10^8\ V \cdot m^{-1})$. On the other hand, a larger $\Delta\mu$ value has been observed for CO molecules bound to the heme iron atom (2.4 $cm^{-1}/(10^8\ V \cdot m^{-1})$)[2] or those chemisorbed on a Pt(111) metal surface (1.0-2.8 $cm^{-1}/(10^8\ V \cdot m^{-1})$).[6, 11-12] Computational studies have reported $\Delta\mu$ values consistent with the experimental observations within the uncertainty of local field correction: 0.43 $cm^{-1}/(10^8\ V \cdot m^{-1})$ for free CO[8] and 1.3 $cm^{-1}/(10^8\ V \cdot m^{-1})$ for heme-CO.[9] In the present study, we explore the VSE in crystalline solid CO. We apply a uniform DC electric field with a magnitude of up to $2.6 \times 10^8\ V \cdot m^{-1}$ to a crystalline CO film, expected to be in its α-phase, by using the ice film nanocapacitor method.[13] The VSE displayed by the CO crystal was examined through reflection-absorption infrared spectroscopy (RAIRS) measurements of the samples.

The effect of an external electric field on molecular crystals has been a subject of considerable interest in fundamental research and technological applications. For example, extensive studies have been done for the realignment and structural change of liquid crystals by an external electric field with important applications for electro-optical devices,[14-15] as well as for materials with strongly correlated electrons which exhibit interesting electrodynamic properties, such as unconventional superconductivity and very large magnetoresistance.[16] The effects of electric fields on molecular crystals may reach a wider variety of properties, including the structure, dynamics, and synthesis of materials. Yet, study of these effects is only in its infancy. For example, the change of crystal structure by the head-to-tail inversion of molecular dipoles has not yet been examined under the influence of an external electric field, mainly because of a high energy barrier for dipole inversion in a crystalline lattice. In the case of amorphous solids, it has been reported that an external electric field with a strength of $10^8\ V \cdot m^{-1}$ can reorient small polar molecules like acetone and chloroethane by certain angles toward the direction of the applied field.[17-18] CO is an attractive candidate to explore the possibility of dipole inversion in a crystalline solid because, while the molecule is a heteronuclear diatomic, it has a very small permanent dipole moment (0.112 Debye), yielding a weak dipole-dipole (μ-μ) interaction energy (-19 $J \cdot mol^{-1}$) in the α-phase CO crystal.[19] In the CO crystal, individual CO molecules at each lattice site have two possible head-to-tail

orientations, and the distribution between the two relative orientations is almost random because of the weak μ-μ interaction.[19-21] The disordered orientational distribution is retained upon cooling of a CO crystal towards absolute zero degree because the kinetics of the ordering process are extremely slow at low temperatures, resulting in a residual molar entropy of approximately $R\ln 2$.[22] The present experiment explores the effect of a strong external electric field on dipole inversion in the CO crystal.

Intermolecular μ-μ interactions in a thin film of cubic crystalline CO couple the intramolecular CO stretching vibrations, resulting in the degeneracy of the E modes and of the A mode collective vibrations to be lifted as a result of mixing and the corresponding spectral features to split into longitudinal optical (LO) and transverse optical (TO) modes.[23-25] IR spectroscopic studies have revealed that the relative intensity, as well as the splitting between the spectral features assigned to LO and TO modes in condensed CO samples, depend on their temperature, on their morphology (*i.e.*, film thickness, crystallite size and shape), and on their structure (*i.e.*, amorphous or crystalline, defects, orientational disorder). Also, as the transition dipoles for the LO and the TO modes are orthogonal to one another, their relative intensities in the RAIR spectra of CO films vary strongly with the incidence angle as well as with the polarization of the infrared light.[23-29] For example, the intensity of the LO feature in RAIR spectra of CO films is modulated very strongly by changes in incidence angle thereby indicating that the LO mode couples with p-polarized light. It also reveals that its transition dipole polarization is parallel to the surface normal.[25] The dependence of the LO-TO splitting on the growth temperature of CO films has also been examined. Its magnitude was interpreted in terms of the VSE originating from the internal electrostatic field developed during film growth.[28]

However, we stress that the interpretation of VSE from the RAIR spectra of thin solid CO films obtained at grazing incidence in the reflection-absorption geometry requires special attention due to optical effects (refraction and anomalous dispersion, optical interferences between the multiple reflections at the film-vacuum and film-substrate interfaces yielding standing waves within the film, etc). Indeed, these trivial optical effects were shown to strongly affect the splitting of the spectral features assigned to LO and TO modes in solid CO films adsorbed on nitrogen spacers, as well as their relative intensities, phenomena that were described very satisfactorily by M.E. Palumbo *et al.* using a simple classical optics model.[27] In the present work, we describe the optical effects on RAIR spectra also using classical optics for the investigation of VSE in solid CO films under the influence of an external electric field. This allows the magnitude of the VSE on the frequency and intensity of the spectral features assigned to LO and TO to be quantitatively assessed. The behavior of the intramolecular CO stretching band of crystalline CO is compared and contrasted with that of amorphous CO, providing evidence that the external electric field affects collective vibrational excitations in

solid CO in a qualitatively different way than it does localized vibrational excitations. Further evidence is garnered by comparing and contrasting the VSE displayed by collective LO and TO modes in solid CO with that displayed by the localized molecular vibrations of $^{13}C^{16}O$ and $^{12}C^{18}O$ minor isotopologues that are vibrationally decoupled from the lattice phonon.

2. Experimental Method

The experiment was carried out in an ultrahigh-vacuum (UHV) surface analysis chamber,[6] which was equipped with a low-energy Cs^+ ion gun, a Kelvin work-function probe, a quadrupole mass spectrometer (QMS), and a Fourier transform infrared (FTIR) spectrometer. The sample comprised of stacked layers of H_2O, Kr, CO, Kr, and H_2O films grown in sequence by vapor deposition on a Pt(111) single-crystal substrate cooled by a closed-cycle He refrigerator. The Kr and H_2O films were sequentially grown at 10 K by backfilling the chamber with the corresponding gases. The CO layer was then deposited at 20 K, a temperature at which crystalline CO in the α-phase is known to form,[28, 30] by introducing CO gas through a tube doser in order to reduce contamination of the chamber walls. The resultant CO film was most likely polycrystalline. The orientational distribution of CO molecules in the polycrystalline sample was expected to be isotropic due to the averaging effect over different domains of α-phase microcrystals. To compare the results for crystalline and amorphous CO samples, an amorphous CO layer was prepared in selected experiments by reducing the deposition temperature to 10 K. Kr (99.999%) and CO (99.95% purity) gases were used as purchased. Distilled liquid water was used after degassing through freeze-pump-thaw cycles.

The electric field was applied across the sample by using the ice film capacitor method.[13] In this method, Cs^+ ions generated from a low-energy Cs^+ ion gun were soft-landed on the surface of the topmost H_2O layer of the sample, thereby uniformly charging its surface with positive charge and drawing the same amount of negative charge at the metal substrate surface to form a nano-sized capacitor with dielectric spacers. The resultant voltage (V) across the sample was measured using a Kelvin work-function probe. The electric field was estimated from measurements of the voltage and thickness of the sample. For samples composed of multiple stacked layers of different dielectric films, the electric field strength applied to the solid CO layer can be estimated using equation 1:[31]

$$F = \frac{V}{d_{CO} + d_{\underline{Kr}}\frac{\varepsilon_{CO}}{\varepsilon_{\underline{Kr}}} + d_{H_2O}\frac{\varepsilon_{CO}}{\varepsilon_{H_2O}}} \quad (1)$$

where V is the voltage across the whole film, and d_{CO}, $d_{\underline{Kr}}$, and d_{H_2O} are the thicknesses of corresponding layers. ε_{CO}, $\varepsilon_{\underline{Kr}}$, and ε_{H_2O} are relative permittivities, which have the values of

1.8,[21] 1.8,[32] and 2,[33] respectively, at the temperature at which the experiments were performed. The thicknesses of the constituent layers were estimated from temperature-programmed desorption (TPD) measurements.

RAIRS measurements were conducted using a commercial Fourier-transform infrared (FTIR) spectrometer (Bruker, Vertex 70). The incident IR beam was p-polarized by resorting to a wire grid polarizer, focused onto, and reflected from, the Pt(111) substrate at a grazing incidence angle of approximately 85° and finally, refocused and detected by a mercury-cadmium-telluride detector located outside the UHV chamber. In this experimental geometry, the direction of the light polarization was nearly parallel to that of the applied DC electric field. The IR spectra were obtained by scanning 256 times with a resolution of 1 cm^{-1}. RAIRS spectra were acquired at a sample temperature of 10 K, unless specified otherwise.

RAIR spectra were modeled by calculating the reflectivity of the substrate (R_S) and of the composite film/substrate system ($R_{F/S}$) for p-polarized light enabling simulations of the absorbance ($A = -\log[R_{F/S}/R_S]$) for the composite films to be performed. In the simulations, the optical constants reported by Palumbo *et al*. were used for CO (with an optical index of refraction, $n_\infty = 1.26$),[27] those from Plessis *et al*. were used for ASW (with $n_\infty = 1.28$),[34] while Kr and Ar were treated as a transparent substance (with $n_\infty = 1.38$ for Kr and $n_\infty = 1.291$ for Ar) in the spectral range of interest for this work. Adjustments were made in the model parameters, *viz*., the angle of incidence (81±1°) and layer thicknesses (8.1 nm, 22.4 nm and 24.0 nm for H_2O, Kr, and CO, respectively, for a crystalline CO sample, and 16.1 nm, 34.2 nm, and 76.3 nm for H_2O, Ar, and CO, respectively, for an amorphous CO sample), until the best agreement of the simulated RAIR spectra with experiment was achieved.

3. Results and Discussion

3-A. Stark-Effect Spectra of Crystalline CO Films

Figure 1 shows an expanded view of the intramolecular CO stretching frequency region of a RAIR spectrum from a sample composed of a polycrystalline α-CO layer. The strongest peak at 2142 cm^{-1} was previously assigned[23-25] to the LO mode of $^{12}C^{16}O$ in crystalline CO and the shoulder peak at 2138.5 cm^{-1}, to the corresponding TO mode. Additional weak absorption features appear near these peaks, which include a shoulder peak at 2135 cm^{-1} due to CO impurities trapped within the Kr film,[35] and broad absorptions near 2150 cm^{-1} due to CO interacting with H_2O (*i.e*., CO molecules trapped within or adjacent to the H_2O film).[36] The peaks due to the minor isotopologues, $^{13}C^{16}O$ and $^{12}C^{18}O$, appear at 2092.2 and 2088.5 cm^{-1}, respectively.[37] The $^{13}C^{16}O$ and $^{12}C^{18}O$ bands have distinctly different spectral shapes from the LO-TO bands as a result of decoupling of the $^{13}C^{16}O$ and $^{12}C^{18}O$ stretching vibrations from

those of the $^{12}C^{16}O$ isotopologues, from which they are well separated in frequency. In the text to follow, the vibrationally decoupled $^{13}C^{16}O$ and $^{12}C^{18}O$ bands will be referred to as the molecular CO bands, and the LO-TO bands of $^{12}C^{16}O$ in crystalline CO will be referred to as the solid CO bands. Also, for simplicity, the mass number will be omitted for the most abundant ^{12}C and ^{16}O isotopes. The corresponding spectrum from a sample composed of an amorphous CO layer is shown in Fig. S1 of Supporting Information for comparison with that from a sample composed of a crystalline CO layer.

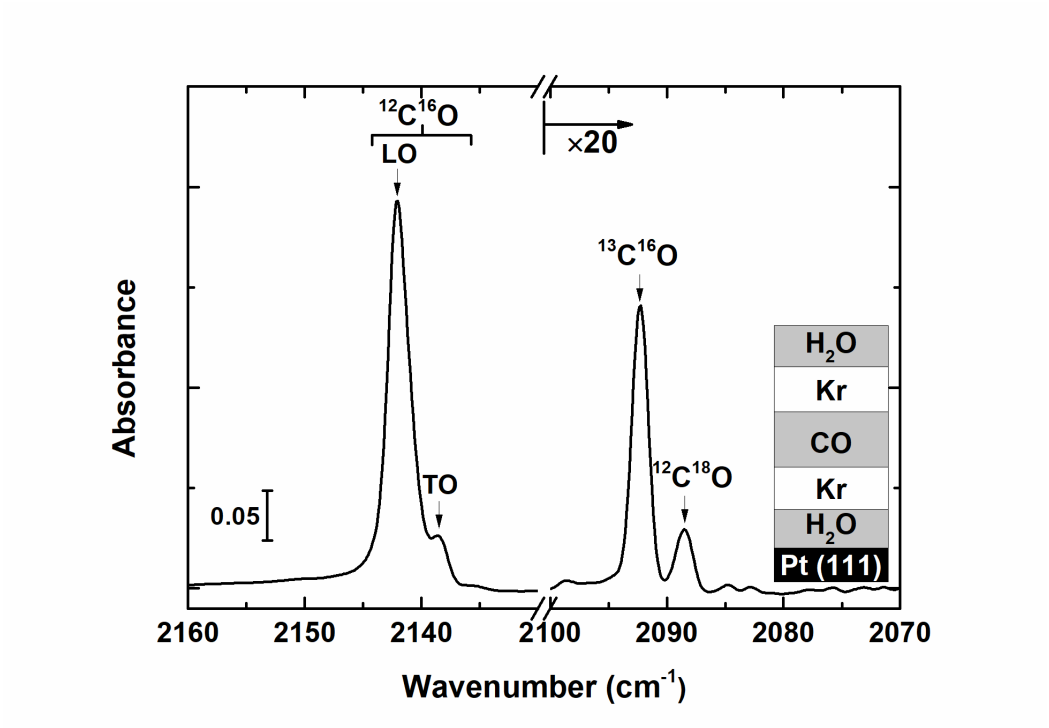

Figure 1. Expanded view of the RAIR spectrum from the composite film schematically drawn in the inset. The crystalline CO layer (thickness of 53 ± 5 nm) is sandwiched between a pair of Kr layers (48 ± 3 nm each) and H_2O layers (17 ± 1 nm each). The most intense features are assigned to the LO and TO modes resulting from collective vibrational excitations of $^{12}C^{16}O$ in the crystalline CO lattice. The molecular CO bands resulting from vibrational excitation of the minor isotopologues ($^{13}C^{16}O$ and $^{12}C^{18}O$) are shown magnified by 20 times.

An external electric field was applied across the composite film by charging the ice nanocapacitor with Cs^+ ions. The applied electric field strength was increased by increasing the amount of Cs^+ ions deposited onto the top H_2O layer of the capacitor, and it was decreased by spraying low-energy electrons onto the Cs^+-deposited H_2O surface. The field-dependent

variations of the solid CO bands, and of the molecular CO bands, are presented in Figure 2. Figure 2(a) shows the evolution of the spectra observed during the increase of the electric field up to the highest field strength of 2.4×10^8 V·m^{-1}, whereas Figure 2(b) shows those observed while subsequently decreasing the field strength. In Figure 2(a), the increase of the electric field to moderate strengths broadens the molecular CO bands. At high fields, each of the molecular CO band splits into two peaks thereby creating a dip at the frequency of the field-free oscillators. In the case of the solid CO bands, the electric field not only increases the band width, but it also changes its peak position and intensity. The main features of these spectral changes have been observed to be reversible with respect to an increase or a decrease in field strength.

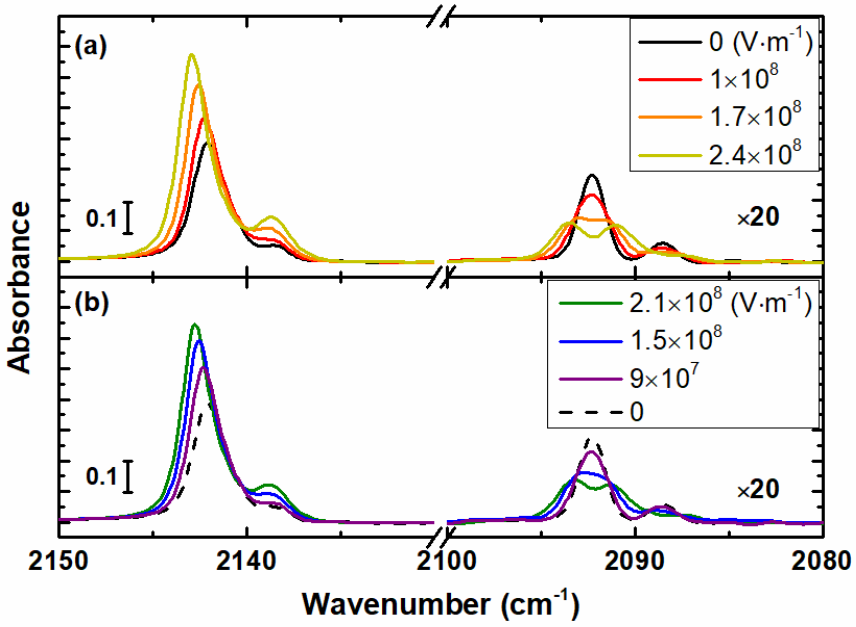

Figure 2. Expanded view of the RAIR spectra that show the effect of the external electric field on the solid CO band and on the molecular ^{13}CO and C^{18}O bands of crystalline CO. (a) Spectra obtained during the increase in field strength. The rainbow color code indicates increasing field strengths, in the sequence from black to gold. (b) Spectra obtained during the decrease in field strengths, in the sequence from green to violet, after reaching the highest field strength [i.e., the gold spectrum in (a)]. The black-dash trace in (b) is the zero-field spectrum reproduced from (a). The ^{13}CO and C^{18}O bands are magnified 20 times. The baselines are corrected numerically. All the spectra were acquired from the same sample at 10 K.

Figure 3 graphically summarizes the field-dependent changes for the molecular CO and solid CO bands. Figure 3(a) shows that, while the integrated absorbance of the solid CO band, normalized to that of the field-free sample, increases as the electric field strength increases, that of the molecular CO bands remains constant. Figure 3(b) reports the peak position of the solid CO band as a function of field strength. The LO band peak position exhibits a unidirectional blue-shift with increasing field strength. The TO band peak position changes with the field strength but only marginally and within the experimental uncertainty (not shown). The data points obtained during the field increase and decrease nicely overlap with each other, indicating that these field-dependent changes are reversible.

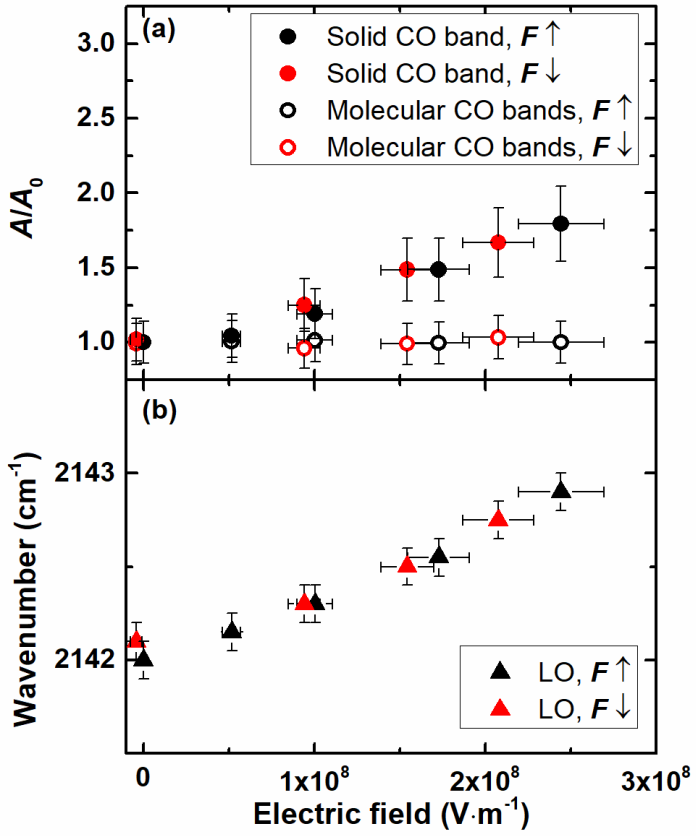

Figure 3. (a) Plot of the integrated absorbances of the solid and molecular CO bands versus applied electric field strength. The absorbances are normalized (A/A_0) to those measured at zero electric field (A_0). Filled circles display the behavior observed for the solid CO band, while open circles display the corresponding trend for the molecular CO bands. Black and red color

codings indicate data points obtained during the increase and decrease in field strength, respectively. (b) Plot of the peak positions of the LO band versus field strength. The LO peak positions (triangles) are read at the intensity maxima of each spectrum without deconvolution. All data points are measured from the spectra presented in Figure 2. The error bars represent the instrumental uncertainties.

In addition to the changes mentioned above, the shape of the molecular CO bands becomes slightly asymmetric as the electric field strength increases. That is, when the molecular CO band splits into two peaks at high field strengths (Figure 2), the blue-shifted component has stronger intensity than the red-shifted component. This asymmetrization of the spectral shape has been observed to be irreversible with respect to the increase or decrease of field strength. This behavior will be discussed in more detail in Section 3D.

3-B. Spectral Analysis of Molecular CO Bands

Since molecular ^{13}CO and $C^{18}O$ bands are vibrationally decoupled from the lattice phonons, their Stark-effect spectrum may be understood in terms of changes of individual molecular properties in presence of the electric field. Indeed, the spectral broadening and splitting of the molecular CO bands in the electric field observed in Figure 2 can be understood as the VSE on isotropically orientated, independent oscillators, as explained in previous studies.[6, 38] That is, when the p-polarization vector of incident IR beam is parallel to the direction of the applied electric field, oscillators that are oriented parallel or anti-parallel to the applied field direction experience a large Stark frequency shift, while those perpendicular to the field do not. In addition, the oscillators that are perpendicular to the field do not contribute to the spectral absorbance. As a result, a dip is created at the center of the spectral profile at high field strength.

Despite the change in spectral profile, the absorbance of the molecular CO bands does not change with electric field strength (Figure 3a). This indicates that the angle of alignment of CO dipoles with respect to the applied field direction does not change. Reorientation of CO molecules toward the applied field direction would have increased the spectral absorbance. On the other hand, the spectral shape of molecular CO bands becomes asymmetric at high field strength. The asymmetrization indicates that the average orientation vector of transition dipole moment leans toward the direction of the applied field (or the light polarization), thereby breaking the balance between the populations of red and blue-shifting oscillators. These two seemingly contradictory observations can be explained by the flip motion of CO dipoles. The head-to-tail inversion of CO at the lattice sites, driven by electrostatic interactions between the dipole and the electric field, increases the average angle of *orientation* of the permanent electric

dipole moment (and of the transition dipole moment), while maintaining the angle of *alignment* constant. This results in the asymmetric profile and constant absorbance of molecular CO bands as a function of increasing electric field.

At the applied field strength of 1×10^8 V · m^{-1}, the dipole-field interaction energy ($\mu \cdot F = -23$ J · mol^{-1}) is comparable in magnitude to the dipole-dipole interaction energy (–19 J · mol^{-1}) in the lattice.[19] Therefore, the field-induced inversion of CO may become energetically feasible. The flip motion of CO molecules in the crystal, rather than its reorientation by continuous angle, is consistent with the observations reported by nuclear magnetic resonance[39] and nuclear quadrupole resonance experiments.[40] One might consider that the asymmetric shape of the molecular CO bands results from the VSE that changes both the frequency and intensity of the vibrational transitions.[7] However, the irreversible nature of the asymmetrization of the spectral shape with respect to the change of applied field supports that it is due to a structural response to the external field (inversion) rather than an electronic response (VSE).

Based on these considerations, we have simulated the field-dependent changes of the molecular CO bands using a model that accounts for the simultaneous vibrational Stark shift in CO frequency and the inversion of CO molecules in the crystalline CO lattice, as described below. The shift in vibrational frequency ($\Delta\tilde{\nu}$) for isolated oscillators due to the Stark effect can be expressed by eq 2.[38]

$$\Delta\tilde{\nu} \cong -\left(\Delta\mu \cdot F + \tfrac{1}{2}F \cdot \Delta\alpha \cdot F\right) \qquad (2)$$

where F is the electric field, $\Delta\mu$ is the Stark sensitivity factor (or Stark tuning rate) representing the difference in dipole moments between the ground and excited vibrational states, and $\Delta\alpha$ is the difference in their polarizabilities. The numerical simulation of a spectrum resulting from an ensemble of oscillators is described in Supporting Information and in previous reports.[41] In brief, the spectrum is constructed from the summation of the absorbances (A) from individual oscillators considering two angular dependency factors: (i) $A \propto \cos^2\theta$, where θ is the angle between the transition dipole moment of individual oscillators and the p-polarization direction of light, and (ii) the Stark frequency shift proportional to $\cos\gamma$, where γ is the angle between the difference dipole $\Delta\mu$ and F. In the present experimental geometry, θ and γ are equal.

To simulate the field-induced inversion of CO, we randomly select a certain number of oscillators whose molecular dipole moment is oriented against the direction of applied electric field, and their direction is inverted by 180°. This procedure shifts the population of red- and blue-shifting oscillators and asymmetrizes their relative intensities, while maintaining their total absorbance invariant. The number of flipped oscillators is adjusted until the asymmetry

of experimental spectrum is satisfactorily reproduced.

In Figure 4, the zero-field molecular CO features (top) are fitted by two Gaussian curves representing the initial random orientation of ^{13}CO and $C^{18}O$ molecules. The spectra at intermediate (middle panel) and strong (bottom panel) field strengths are simulated by including the vibrational Stark shift and the dipole inversion, as described above. The simulations reproduce the major features of the experimental spectra quite well, including the peak splitting and asymmetrization. The spectral fitting was adjusted using the values of $|\Delta\mu|$, $|\Delta\alpha|$, and the fraction of dipole-inverted CO. In this procedure, the VSE contribution from $\Delta\mu$ dominates the frequency shift of oscillators as a function of external field strength, which is responsible for the peaks broadening and for their splitting. The remaining two factors contribute to the asymmetry in the peak shape.[38] However, it is observed that the contribution from $|\Delta\alpha|$ is negligible compared to that of CO inversion. At the highest field strengths (bottom panel), the experimental spectral profile is slightly broader than the simulated profile. This discrepancy is probably related to the inhomogeneity in electric field strength within the local environment of the lattice, even when the external electric field is uniform.[41] From the results of fitting the simulated spectra to the experimental ones, we estimate the Stark sensitivity factor ($\Delta\mu = \Delta\tilde{\nu}/F$) of ^{13}CO and $C^{18}O$ to be 0.69 ± 0.05 $cm^{-1}/(10^8 V \cdot m^{-1})$. This value for isolated CO molecules in crystalline CO is close to $\Delta\mu = 0.6\text{-}0.7$ $cm^{-1}/(10^8 V \cdot m^{-1})$ obtained for CO embedded in amorphous solid water[6] or frozen THF films.[3] The similar Stark sensitivity factors for CO in different solid matrices imply that the local field correction is relatively invariant to the nature of the matrix at low temperature because it arises mostly from electronic polarizability effects. Also, with reference to $\Delta\mu = 0.43$ $cm^{-1}/(10^8 V \cdot m^{-1})$ for free CO determined by *ab initio* calculations,[8] the local field correction factor in the matrix is estimated to be about 1.6.

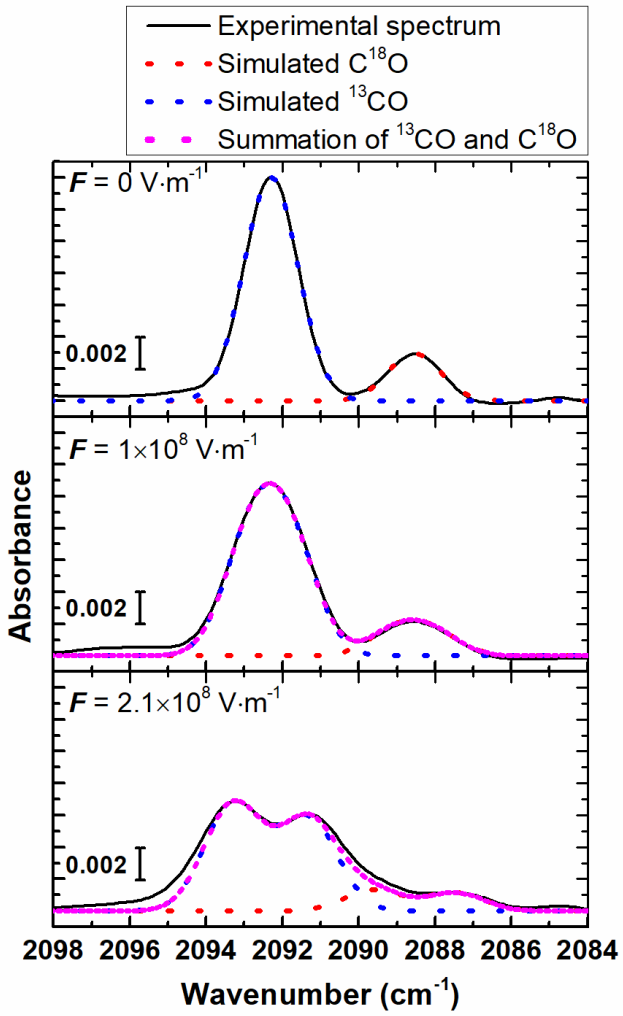

Figure 4. Spectral simulation of the VSE on the molecular CO bands. (Top panel) Fitting of the ^{13}CO and $C^{18}O$ bands at zero electric field with two Gaussians. (Middle panel) Fitting results at a moderate field strength (1.0×10^8 V · m^{-1}) obtained by including the effects of the frequency shift from VSE along with the inversion of a fraction of the CO molecules in the crystalline CO lattice. (Bottom panel) Fitting results at a high field strength (2.1×10^8 V · m^{-1}). The high field spectrum clearly shows asymmetric absorbances of the red- and blue-shifted components of the ^{13}CO band. The black traces are the experimental spectra, the blue dotted traces are the simulated spectra for ^{13}CO, the red dotted traces are the simulated spectra for $C^{18}O$, and the magenta dotted traces are the summations of red- and blue-dotted traces.

According to the observation that the intensity of the blue-shifted component of the molecular CO band increases at higher field strengths, it is concluded that field-oriented CO molecules exhibit a blue-shift in their vibrational frequency. However, because the μ and $\Delta\mu$ vectors point in the same direction for the great majority of simple polar molecules, electric

field-induced orientation of chromophores usually results in a red-shifted vibrational frequency. Therefore, this unique behavior is evidence that the μ and $\Delta\mu$ vectors point in opposite directions for CO molecules in crystalline CO, a behavior similar to those predicted theoretically for free CO.[7] For comparison, when an external electric field is applied in the direction from O to C, for example for the oriented chemisorbed CO layer on a Pt metal surface,[6] the CO molecules exhibit a red-shift in their vibrational frequency. This observation, together with the fact that the field-induced orientation of CO molecules in crystalline CO results in a blue-shifted vibrational frequency, further supports the fact that the dipole moment vector in CO points from C to O (*i.e.*, $C^{\delta-} \equiv O^{\delta+}$). Finally, quantitative analysis of the asymmetric profile of the molecular CO bands estimates that 6-9% of CO molecules in the crystal are dipole-inverted by their interaction with the external electric field at $F = 2.1 \times 10^8$ $V \cdot m^{-1}$.

3-C. Simulations of RAIR Spectra

Figure 5a compares the optical parameters (blue and green trace for the real, $n(\omega)$, and imaginary, $k(\omega)$, parts of the index of refraction, respectively, as a function of wavenumber, ω) reported by Palumbo et al.[27] with the experimental (Figure 5b: black trace) and simulated (Figure 5b: red trace) RAIR spectra in the spectral range of interest. We stress that the extent of crystallinity of the samples from which the optical constants were obtained is uncertain.[42] One notices that the molecular CO bands (2085-2100 cm^{-1}) in the RAIR spectra are quite similar in shapes and positions to those expected from the corresponding features in the frequency-dependent extinction coefficients, $k(\omega)$ (Figure 5a; green trace). In contrast, both the shape and position of the solid CO bands (2135-2145 cm^{-1}) are strongly perturbed in the RAIR spectrum and thus share very little similarities with those of the corresponding feature in $k(\omega)$ (Figure 5a: green trace). These differences are attributed to trivial optical effects that are well-known to distort absorbance spectra in the reflection-absorption geometry. They should not, however, be confused with the band splitting arising from LO-TO couplings that are responsible for the broadening and the intensity distribution within the spectral feature attributed to the coupled CO stretching vibrations of solid CO in $k(\omega)$ shown in Figure 5a (green trace). Indeed, anomalous dispersion in the vicinity of the strong absorption CO stretching feature (especially in the range where $n<1$) is responsible for the significant blue-shift (i.e., 4-5 cm^{-1}) in the absorbance maximum (Figure 5b; black trace) compared with the maximum in $k(\omega)$ (Figure 5a; green trace). A quantitative understanding of these trivial optical effects is essential to provide an accurate interpretation of the splittings and shifts in spectral features due to vibrational Stark effect in solid CO by distinguishing its effects from those arising from LO-TO couplings.

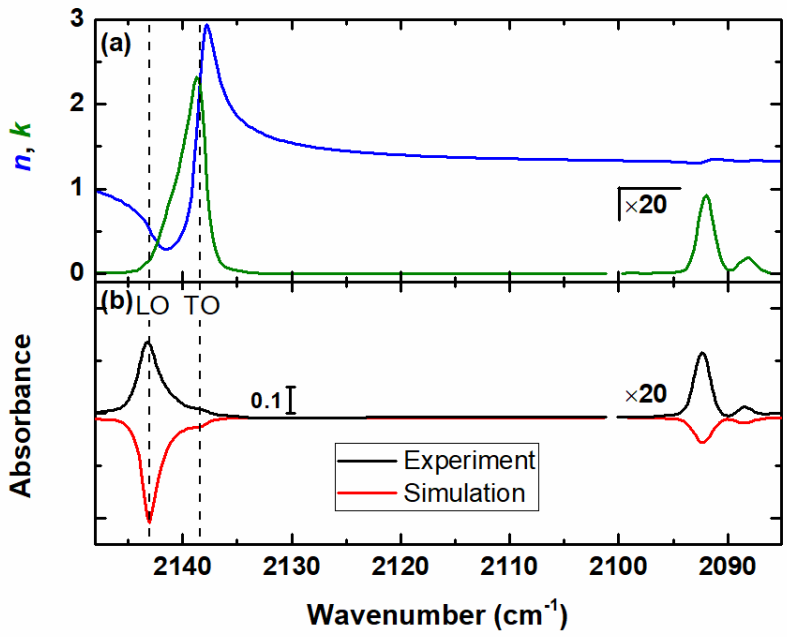

Figure 5. (a) The real [$n(\omega)$: blue trace] and imaginary [$k(\omega)$: green trace] parts of the complex index of refraction for solid CO from Palumbo et al.[27] used in the simulations of the RAIR spectra of composite films in absence of an applied external electric field; (b) zero-field experimental (black trace) and simulated (red trace, upside down) RAIR spectra. The vertical dashed lines indicate the frequencies of the LO and TO modes reported for solid CO.[43]

In Figure 6, the simulated RAIR spectra for various selected external electric fields (b) are compared with the experimental RAIR spectra (a). The simulation of the Stark-effect spectra uses a simple model that describes the CO crystal as being composed of two types of oscillators, one oriented parallel and the other anti-parallel to the electric field. Their relative abundance is determined experimentally from the degree of asymmetry displayed by molecular CO band shape described in Figure 4, providing a measure of the fraction of CO molecules that reorient as a function of the external electric field. The extinction coefficient of the samples in the presence of the field, $k(\omega)$, is described as the summation of two components, both following the form reported by Palumbo et al.,[27] one blue-shifting and the other red-shifting due to VSE. The real part of the index of refraction, $n(\omega)$, is then calculated using the Kramers-Krönig relation[42] enabling the effect of the external electric field on the RAIR spectra of composite films to be modeled. In the molecular CO spectral range (2085-2100 cm^{-1}), the simulated RAIR spectra reproduce the experimental spectra very satisfactorily. However, while the simulated

RAIR spectra qualitatively reproduce the shifts in band positions in solid CO spectral range (2135-2150 cm^{-1}) as a function of the magnitude external electric field, they do not capture the trends in peak intensity observed experimentally. The large increases in absorbance displayed by the collective solid CO vibrational excitations may reveal the fact that their transition moments are enhanced, as a result of their interaction with the external electric field, compared to that of localized molecular CO vibrational excitations. Modeling the collective vibrational excitations, such as demonstrated for CO aerosols by Firanescu and Signorell,[42] could elucidate how the external electric field affects their intensity.

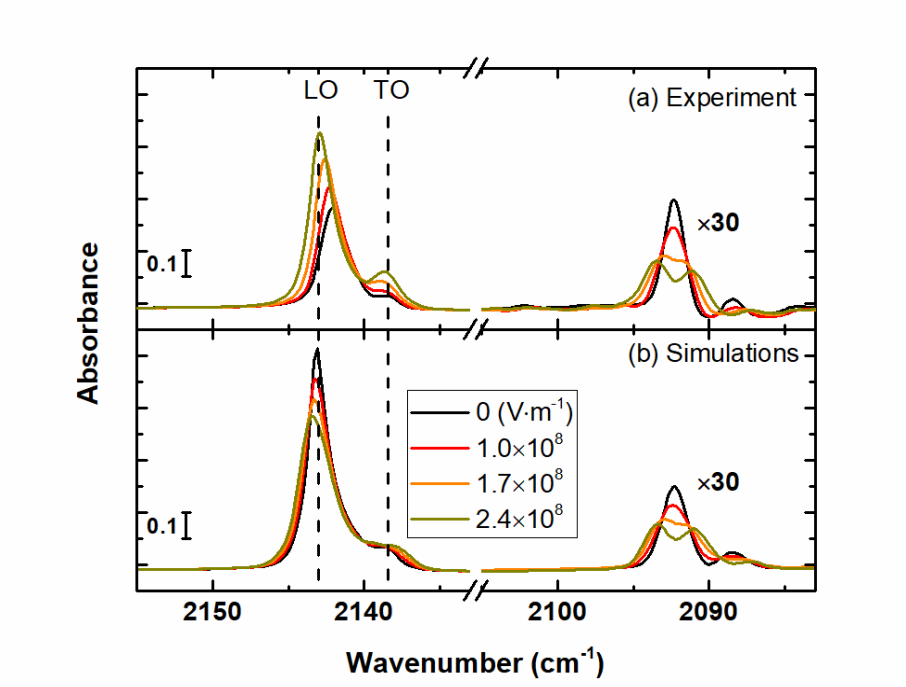

Figure 6. Expanded view of the RAIR spectra that show the effect of the external electric field on the solid CO band, and on the molecular ^{13}CO and $C^{18}O$ bands, of crystalline CO: (a) Experimental spectra obtained during the increase in external electric field strength (reproduced from Figure 2a); (b) Simulations of the experimental RAIR spectra using a simple classical optics model (see text for details).

If the externally applied field impacts so strongly the collective CO stretching vibrational excitations in the ordered lattice of crystalline CO, this effect might be suppressed to some extent in the highly disordered and defective lattice of amorphous CO. Indeed, Figure 7 shows that the Stark-effect spectra of amorphous CO display a qualitatively different behavior compared to that of a crystalline CO film (Figure 6). In this experiment, the amorphous CO

layer was prepared by vapor deposition at 10 K but otherwise, the same sample preparation protocol described above for crystalline CO samples was followed. In the experimental spectrum at zero field (Figure 7a; black trace), the widths of molecular and solid CO bands are broader for amorphous CO than for crystalline CO (Figure 6a; black trace). Furthermore, the applied external electric field shifts the spectral features to a much greater extent but also, it changes their band profiles in a qualitatively different fashion than the behavior displayed by the crystalline CO samples. Notably, the external electric field does not increase the intensity of the solid CO band in amorphous CO significantly (Figure 7a), in contrast to the sizable increase of its intensity displayed by crystalline CO (Figure 6a).

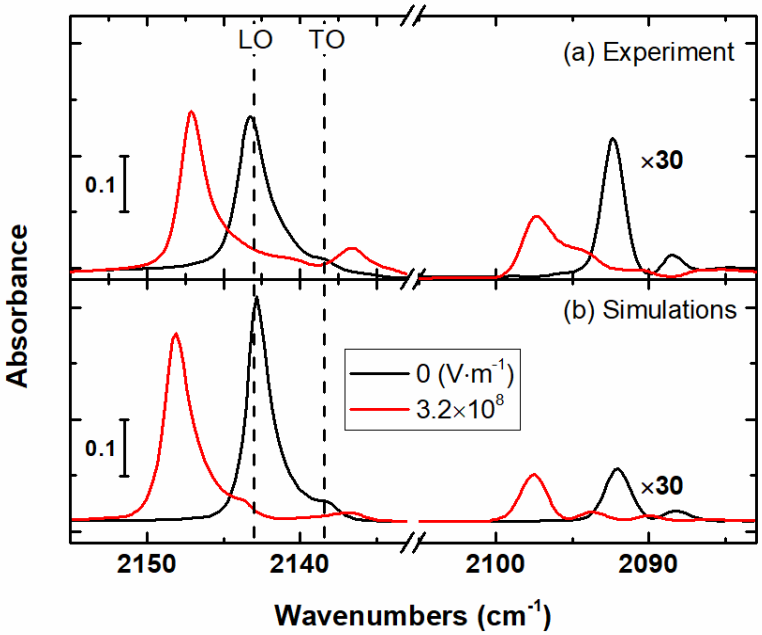

Figure 7. Expanded view of the RAIR spectra that show the effect of the external electric field on the solid CO band, and on the molecular ^{13}CO and $C^{18}O$ bands, of amorphous CO. (a) Experimental spectra obtained for field strength of 0 and 3.2×10^8 V · m^{-1}. (b) Simulations of the experimental RAIR spectra using a simple classical optics model (see text for details).

The same simulation protocol described above for crystalline CO was also used for amorphous CO samples. Spectral simulations for samples composed of an amorphous CO layer produce a much better agreement with the experimental results (Figure 7), especially as regards the evolution of the intensities and position of the molecular CO and of the solid CO spectral features as a function of increasing electric field as well as the changes in their band shapes.

Clearly, while our classical optics simulations provide a satisfactory account of the effect of the external electric field on localized vibrations (i.e., molecular CO bands in both crystalline and amorphous CO samples, as well as solid CO band in amorphous CO samples), they unfortunately fail to describe the increasing intensity of the solid CO band in crystalline CO as a function of the external electric field.

From the comparison of the behavior displayed by crystalline and amorphous CO, in the molecular CO and solid CO spectral ranges, it is inferred that the sizable increase in intensity of the solid CO band for crystalline CO subjected to an external electric field is related to the long-range order and intermolecular μ-μ couplings in the ordered periodic lattice of crystalline CO.[42] In general, an external electric field can change vibrational frequencies of isolated chromophores as well as the intensity of vibrational transitions.[7] However, our results show that the intensities of molecular CO bands (Figure 3a), resulting from vibrational excitations of individual localized oscillators, are not significantly changed by an external electric field of the magnitude of the present experiment. To some extent, the same conclusion also applies to the solid CO band of amorphous CO. Therefore, we are led to conclude that the increased intensities of the solid CO band in crystalline CO is probably due to the influence of an external electric field on the transition dipoles of the collective vibrational excitations of coupled oscillators in crystalline CO, such as described by Firanescu and Signorell.[42] Understanding the effect of the externally applied field on the intensity and shape of the solid CO spectral features in crystalline CO will be a subject for future theoretical and experimental study.

3-D. Field-Induced Dipole Inversion

The analysis of the asymmetric spectral profile of the molecular CO bands, described in Section 3-B, provides an estimate of the fraction of dipole-inverted CO molecules (*f*) in crystalline CO as a result of their interaction with an external electric field. Figure 8 shows the plot of *f* versus the magnitude of the applied electric field measured experimentally in the following sequence: First, the electric field was increased stepwise from zero to 2.4×10^8 V · m^{-1} by increasing the dose of Cs^+ ions (black circles) then, it was reduced back to zero by spraying low energy electrons (red circles) and then, it was increased again up to 2.3×10^8 V · m^{-1} (blue circles). The graph shows that *f* increased to just over 5% when the field strength was first increased (black circles). However, a strong hysteresis appeared when the field strength was subsequently decreased (red circles). We stress that measurements of *f* were only possible at high fields (*i.e.*, $> 1 \times 10^8$ V · m^{-1}), where VSE causes the splitting of molecular CO bands to be large enough to quantitatively evaluate the asymmetry of the band shapes, which is produced by the asymmetric (dipole-inverted) populations of red- and blue-shifting components, as mentioned above. Accordingly, the magnitude of the hysteresis in *f* could only be obtained reliably at high

fields, while the behavior at low fields ($\leq 1 \times 10^8$ V · m^{-1}) was extrapolated from the high-field behavior (displayed as dashed red and blue lines, for the decreasing and increasing fields, respectively). Nevertheless, extension of the hysteresis down to the weak field region was further supported by observations made during repeated cycles of increasing and decreasing external field. In the second cycle (blue circles), the estimated value of *f* at low field strengths ($\sim 5 \times 10^7$ V · m^{-1}), despite its large uncertainty, was definitely greater than zero and indistinguishable from the high-field values in the previous cycle.

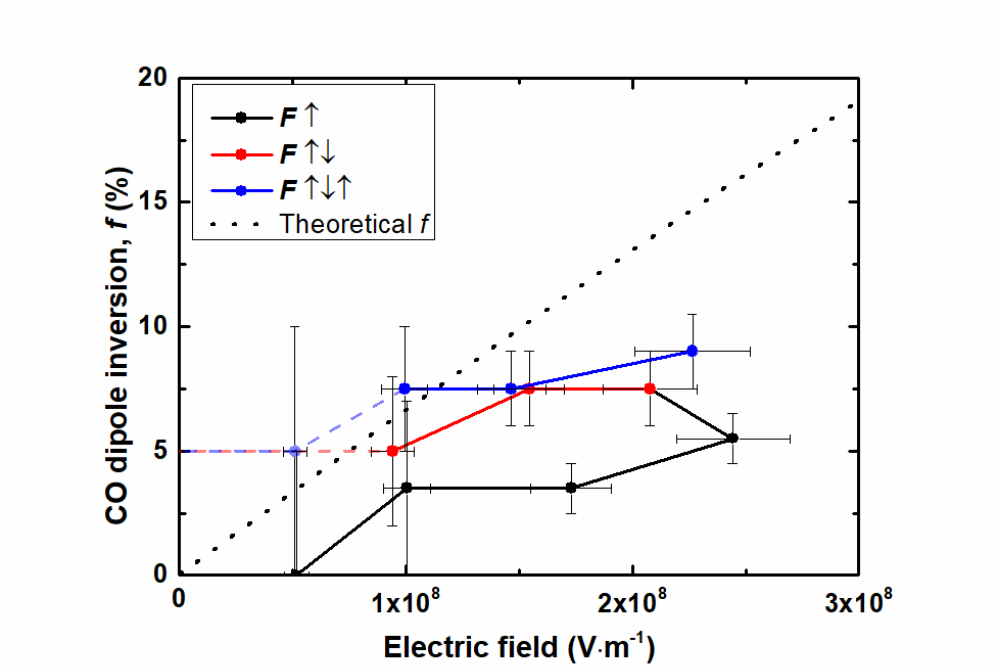

Figure 8. The fraction of dipole-inverted CO molecules (*f* in %) in crystalline CO measured during repeated cycles of increasing and decreasing magnitude of the applied electric field at 10 K. Black circles indicate the values obtained during the increase of the field in the first cycle. Red circles indicate the values obtained during the subsequent decrease of the field, after reaching the highest field strength in the first cycle. Blue circles indicate the values obtained during the subsequent increase of the field from zero in the second cycle, that is after reaching the lowest field strength in the first cycle. The trends in the low field region ($< 1 \times 10^8$ V · m^{-1}) are drawn in dashed lines with the corresponding color codes to highlight the fact that they are extrapolated behaviors. The black dotted line indicates the theoretical prediction of *f* (see text).

The yield of CO inversion in crystalline CO was affected, not only by the magnitude of the electric field applied to the sample, but also by the duration for which the sample was subjected

to the field. We noticed that the field-induced inversion occurred slowly and continually on a timescale similar to that typical for data collection. The slow occurrence of CO inversion, and their effect on *f*, are reflected in the behavior observed during the second leg of first cycle, that is, when the magnitude of the electric field was decreased (red circles in Figure 8). Unexpectedly, *f* was observed to increase, rather than decrease, during the reduction in field strength from 2.4×10^8 V · m^{-1} to 2.1×10^8 V · m^{-1}. During this time interval (~0.5 h), the inversion processes may have continually occurred thereby further increasing *f* in the sample subjected to the external electric fields.

We therefore proceeded to measure the rate of dipole inversion in crystalline CO in the presence of an external electric field. Figure 9 shows a kinetic plot of the inverted portion (*f*) of CO vs the time for which the sample was subjected to the electric field at the strength of $2.6 (\pm 0.2) \times 10^8$ V · m^{-1}. *f* increased continually with time up to about 20% after 8 h. The increase of *f* was fitted assuming first-order kinetics, $f = f_0[1 - \exp(-kt)]$, while the possible occurrence of the reverse process was neglected. Curve fitting gave an estimation of the rate for field-induced CO inversion, $k = 0.22 \pm 0.07$ h^{-1}. In previous studies,[21] the rate for dipole inversion in crystalline α-CO has been measured in the absence of an external electric field at higher temperatures (25-35 K) by means of audio-frequency dielectric measurements. From the Arrhenius behavior of the rates, an activation energy of 6 kJ · mol^{-1} was reported,[21] allowing the dipole inversion rate at zero field of 10^{-16} h^{-1} to be extrapolated down to 10 K. This estimated rate is consistent with our observation of negligible depolarization of crystalline CO at 10 K upon the removal of the external electric field. Compared to the negligibly slow inversion of CO at zero field, the inversion rate of ~0.2 h^{-1} in a strong external electric field represents an enormous increase in inversion kinetics by the applied field. A possible origin of this field enhancement effect may involve non-thermal effects. Indeed, the energetic stabilization due to dipole-electric field interaction is only 0.02 kJ · mol^{-1} at a field strength of 1×10^8 V · m^{-1}, which is smaller than $k_B T = 0.08$ kJ · mol^{-1} at 10 K. This effect will lower the classical barrier height of inversion only by a very small extent, and the associated effect on the increase in inversion rate would be expected to be insignificant. Therefore, the accelerated inversion rate of CO in an external electric field indicates a possible quantum tunneling contribution to the inversion mechanism in crystalline CO. The increase of inversion rate by a factor of ~10^{15} may indicate a significant reduction of the tunneling barrier height by the applied field. This barrier reduction effect may be an interesting subject for future theoretical study.

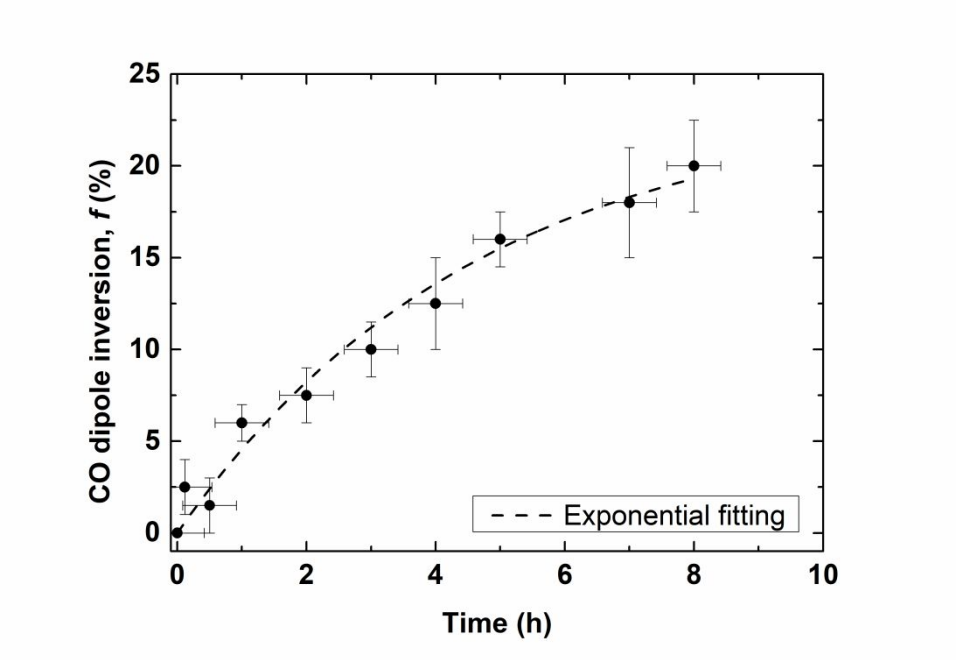

Figure 9. The measurement of dipole inversion (f in %) in crystalline CO as a function of the exposure time to an external electric field strength of $2.6\ (\pm 0.2) \times 10^8$ V · m^{-1} at 10 K. The dashed curve is the exponential function describing first-order kinetics, $f = f_0[1 - \exp(-kt)]$.

A thermodynamic model may be used to estimate the fraction of field-inverted CO molecules in a sample that is at equilibrium with an external electric field. Two contributions are taken into consideration. The first contribution is the enthalpic stabilization gained by dipole inversion in the external electric field. The relative energy (ΔU_F) of a dipole-inverted state under the influence of an external electric field (F) compared to the energy at zero field is calculated by the dipole-field stabilization energy of inverted CO dipoles, $\Delta U_F = 2\mu F\langle\cos\theta\rangle f N_0$, where ΔU_F is $U_F - U_0$, $\langle\cos\theta\rangle$ is the average of $\cos\theta$ of the dipoles whose orientation is against the direction of the applied electric field ($\pi/2 \leq \theta \leq \pi$; their inversion is energetically favored), and N_0 is the total number of CO molecules. The second contribution is the configurational entropy of the CO crystal associated with the two possible orientations of CO at each lattice site. The configurational entropy decreases as the population ratio between "up" (↑) and "down" dipoles (↓) deviates from a random orientation (↑:↓ = 1:1) state. A state where a certain fraction (f) of ↑ is inverted to ↓ has an entropy change that can be estimated using $\Delta S_F = S_F - S_0 = -N_0 k_B[(0.5 + f)\ln(0.5 + f) + (0.5 - f)\ln(0.5 - f) + \ln 2]$, where S_0 is the initial random 1:1 state at zero field and k_B is the Boltzmann constant.

The two contributions, one of enthalpic nature and the other entropic nature, compete one

another to result in an optimal value of f that minimizes the free energy of the CO crystal: $\partial[\Delta U_F(f) - T\Delta S_F(f)]/\partial f = 0$, where T is the temperature. This gives an expression for the equilibrated value of f in an external electric field, which displays the expected Boltzmann distribution (eq. 3).

$$(0.5 + f)/(0.5 - f) = \exp(\mu F/k_B T) \quad (3)$$

The black dotted line in Figure 8 represents this relationship (f = 6.7% at 1×10^8 V · m^{-1} and 16% at 2.4×10^8 V · m^{-1}, using the magnitude of the dipole for free CO molecules), which serves as a reference for interpreting the experimental results. It is noticed that the experimental f values during the increase of the electric field in the first cycle are always lower than those expected from this simple thermodynamic model. The slow occurrence of field-induced dipole inversion precludes the experimental f to reach the thermodynamic f on the timescale of the observations. During the decrease of external electric field, however, the kinetic inhibition causes a pronounced hysteresis, which can result in the experimental f value to be higher than the thermodynamic f value at low fields, as observed in Figure 8. This illustrates the kinetic metastability of a dipole-ordered CO crystal at 10 K. Thermodynamically, a dipole-ordered state in the absence of an external electric field is unstable at 10 K, which is above the Curie temperature (5 K) for crystalline CO. Nevertheless, the depolarization of a CO crystal is kinetically inhibited at 10 K. The observations reported here suggest a method that can generate a dipole-ordered CO crystal by applying a strong external electric field at low temperature.

4. Summary and Conclusions

We have studied the effect of externally applied electric fields on crystalline α-CO films for systematically scanned field strengths up to 2.6×10^8 V · m^{-1}. RAIRS measurements show that the applied electric field reversibly changes the vibrational spectrum of CO films with respect to the change of applied field strength as a result of VSE on the localized CO vibrations and the LO and TO bands of crystalline CO. Irreversible changes are also observed in the molecular CO bands, which are attributed to the inversion of CO orientation at the lattice sites induced by dipole-electric field interactions. Analyses of these spectral changes lead to the following conclusions.

(1) The spectral broadening and splitting of the molecular CO bands in the presence of external electric fields are explained in terms of the VSE on isotropically oriented CO oscillators. VSE analysis of the molecular CO bands reveals a Stark sensitivity factor of 0.69 ± 0.05 cm^{-1}/(10^8 V · m^{-1}) for CO in crystalline solid, which is similar to that of CO embedded in the frozen matrices of H_2O[6] and THF.[3] The field-induced spectral changes

confirm that the vector directions of $\Delta\mu$ and μ are opposite in CO.

(2) The external electric field changes both the shapes and intensities of the LO and TO bands of crystalline CO films. The Stark-effect RAIR spectrum is simulated by using a classical optics model that accounts for the optical effects on the RAIR spectra of thin solid films and the empirical VSE parameters of localized molecular vibrations. The model successfully reproduces the field-induced changes of the molecular CO bands in crystalline and amorphous CO, as well as the solid CO band in amorphous CO, but fails to describe the behavior of coupled CO vibrations in crystalline CO. The results indicate that the field-induced intensity changes for the LO and TO bands are related to the long-range order and intermolecular μ-μ couplings in crystalline CO. Also, it is shown that the inclusion of trivial optical effects in RAIRS is essential for accurate interpretation of the LO-TO features.

(3) The applied electric field facilitates head-to-tail inversion of the dipoles in crystalline CO. The observation is the first example of electric field-control for the inversion of molecular dipoles in a solid crystal, to the best of our knowledge. The dipole inversion occurs with the rate of ~0.2 h^{-1} at the applied field strength of 2.6×10^{8} $V \cdot m^{-1}$ at 10 K, reaching the inversion yield of about 20% in the crystal after 8 h. A dramatic (~10^{15} times) increase in the inversion kinetics by the electric field at 10 K suggests a quantum tunneling contribution to the inversion mechanism. The observed yield for dipole inversion is interpreted in terms of a thermodynamic model that accounts for the energetics of dipole inversion in the external electric field and the resulting changes in configurational entropy of the CO crystal. A strong hysteresis observed during the polarization and depolarization cycle of the CO crystal indicates kinetic metastability of a dipole-ordered state of the crystal at 10 K. The experiment demonstrates that a CO crystal with reduced residual entropy can be formed with the help of an external electric field.

AUTHOR INFORMATION

Corresponding Authors

* To whom correspondence should be addressed. E-mail: Patrick.Ayotte@USherbrooke.ca (P.A.), surfion@snu.ac.kr (H.K.), Tel: +82 2 875 7471, Fax: +82 2 889 8156 (H.K.)

Notes

The authors declare no competing financial interests.

ACKNOWLEDGMENTS

This work was supported by the Samsung Science and Technology Foundation (SSTF-BA1301-04 to H.K.). P.A. acknowledges NSERC (Canada) and MRIF (Québec) for support for this work, and SNU for a prestigious foreign scholar fellowship.

Reference

1. Fried, S. D.; Boxer, S. G., Measuring Electric Fields and Noncovalent Interactions Using the Vibrational Stark Effect. *Acc. Chem. Res.* **2015**, *48*, 998-1006.

2. Park, E. S.; Andrews, S. S.; Hu, R. B.; Boxer, S. G., Vibrational Stark Spectroscopy in Proteins: A Probe and Calibration for Electrostatic Fields. *J. Phys. Chem. B* **1999**, *103*, 9813-9817.

3. Park, E. S.; Boxer, S. G., Origins of the Sensitivity of Molecular Vibrations to Electric Fields: Carbonyl and Nitrosyl Stretches in Model Compounds and Proteins. *J. Phys. Chem. B* **2002**, *106*, 5800-5806.

4. Boxer, S. G., Stark Realities. *J. Phys. Chem. B* **2009**, *113*, 2972-2983.

5. Fried, S. D.; Bagchi, S.; Boxer, S. G., Measuring Electrostatic Fields in Both Hydrogen-Bonding and Non-Hydrogen-Bonding Environments Using Carbonyl Vibrational Probes. *J. Am. Chem. Soc.* **2013**, *135*, 11181-11192.

6. Kang, H.; Shin, S.; Park, Y.; Kang, H., Electric Field Effect on Condensed-Phase Molecular Systems. III. The Origin of the Field-Induced Change in the Vibrational Frequency of Adsorbed CO on Pt (111). *J. Phys. Chem. C* **2016**, *120*, 17579-17587.

7. Hush, N. S.; Reimers, J. R., Vibrational Stark Spectroscopy. 1. Basic Theory and Application to the CO Stretch. *J. Phys. Chem.* **1995**, *99*, 15798-15805.

8. Reimers, J. R.; Hush, N. S., Vibrational Stark Spectroscopy 3. Accurate Benchmark Ab Initio and Density Functional Calculations for CO and CN. *J. Phys. Chem. A* **1999**, *103*, 10580-10587.

9. Dalosto, S. D.; Vanderkooi, J. M.; Sharp, K. A., Vibrational Stark Effects on Carbonyl, Nitrile, and Nitrosyl Compounds Including Heme Ligands, CO, CN, and NO, Studied with Density Functional Theory. *J. Phys. Chem. B* **2004**, *108*, 6450-6457.

10. Chang, S. C.; Weaver, M. J., Coverage-Dependent Dipole Coupling for Carbon Monoxide Adsorbed at Ordered Platinum (111)-Aqueous Interfaces: Structural and Electrochemical Implications. *J. Chem. Phys.* **1990**, *92*, 4582-4594.

11. Mamatkulov, M.; Filhol, J.-S., An Ab Initio Study of Electrochemical vs. Electromechanical Properties: The Case of CO Adsorbed on a Pt (111) Surface. *Phys. Chem. Chem. Phys.* **2011**, *13*, 7675-7684.

12. Luo, J. S.; Tobin, R. G.; Lambert, D. K., Electric Field Screening in an Adsorbed Layer: CO on Pt (111). *Chem. Phys. Lett.* **1993**, *204*, 445-450.

13. Shin, S.; Kim, Y.; Moon, E.-S.; Lee, D. H.; Kang, H.; Kang, H., Generation of Strong Electric Fields in an Ice Film Capacitor. *J. Chem. Phys.* **2013**, *139*, 074201.
14. De Gennes, P.-G.; Prost, J., *The Physics of Liquid Crystals*, 2nd Ed.; Oxford university press: New York, 1993; Vol. 83.
15. Tong, X.; Pelletier, M.; Lasia, A.; Zhao, Y., Fast Cis–Trans Isomerization of an Azobenzene Derivative in Liquids and Liquid Crystals under a Low Electric Field. *Angew. Chem. Int. Ed.* **2008**, *47*, 3596-3599.
16. Tomić, S.; Dressel, M., Ferroelectricity in Molecular Solids: A Review of Electrodynamic Properties. *Rep. Prog. Phys.* **2015**, *78*, 096501.
17. Shin, S.; Kim, Y.; Kang, H.; Kang, H., Effect of Electric Field on Condensed-Phase Molecular Systems. I. Dipolar Polarization of Amorphous Solid Acetone. *J. Phys. Chem. C* **2015**, *119*, 15588-15595.
18. Shin, S.; Park, Y.; Kang, H.; Kang, H., Electric Field Effect on Condensed-Phase Molecular Systems. IV. Conformational Change of 1, 2-Dichloroethane in a Frozen Molecular Solid. *J. Phys. Chem. C* **2017**, *121*, 25342-25346.
19. Melhuish, M. W.; Scott, R. L., Energies of Disorientation in Solid Carbon Monoxide and Nitrous Oxide. *J. Phys. Chem.* **1964**, *68*, 2301-2304.
20. Atake, T.; Suga, H.; Chihara, H., Anomaly in the Heat Capacity of Crystalline Carbon Monoxide at 18 K Associated with Orientational Ordering. *Chem. Lett.* **1976**, *5*, 567-571.
21. Nary, K. R.; Kuhns, P. L.; Conradi, M. S., Head-Tail Disorder and Reorientation in Solid N_2O and CO: Dielectric Study. *Phys. Rev. B* **1982**, *26*, 3370.
22. Clayton, J. O.; Giauque, W. F., The Heat Capacity and Entropy of Carbon Monoxide. Heat of Vaporization. Vapor Pressures of Solid and Liquid. Free Energy to 5000 K. From Spectroscopic Data. *J. Am. Chem. Soc.* **1932**, *54*, 2610-2626.
23. Fox, D.; Hexter, R. M., Crystal Shape Dependence of Exciton States in Molecular Crystals. *J. Chem. Phys.* **1964**, *41*, 1125-1139.
24. Berreman, D. W., Infrared Absorption at Longitudinal Optic Frequency in Cubic Crystal Films. *Phys. Rev.* **1963**, *130*, 2193.
25. Zumofen, G., Calculation of the Vibron Band and of the Vibron–Phonon Combination Bands in the IR and Raman Spectra of Solid α-CO. *J. Chem. Phys.* **1978**, *68*, 3747-3759.
26. Baratta, G. A.; Palumbo, M. E., Infrared Optical Constants of CO and CO_2 Thin Icy Films. *J. Opt. Soc. Am. A* **1998**, *15*, 3076-3085.
27. Palumbo, M. E.; Baratta, G. A.; Collings, M. P.; McCoustra, M. R. S., The Profile of the 2140 cm^{-1} Solid CO Band on Different Substrates. *Phys. Chem. Chem. Phys.* **2006**, *8*, 279-284.
28. Lasne, J.; Rosu-Finsen, A.; Cassidy, A.; McCoustra, M. R. S.; Field, D., Spontaneous Electric Fields in Solid Carbon Monoxide. *Phys. Chem. Chem. Phys.* **2015**, *17*, 30177-30187.

29. Caro, G. M. M.; Chen, Y.-J.; Aparicio, S.; Jiménez-Escobar, A.; Rosu-Finsen, A.; Lasne, J.; McCoustra, M. R. S., Photodesorption and Physical Properties of CO Ice as a Function of Temperature. *A&A* **2016**, *589*, A19.

30. Kouchi, A., Evaporation of H_2O-CO Ice and Its Astrophysical Implications. *J. Cryst. Growth* **1990**, *99*, 1220-1226.

31. Bottcher, C. J. F., *Theory of Electric Polarization*, 2nd Ed.; Elsevier: Amsterdam, NY, 1973.

32. Bacalis, N. C.; Papaconstantopoulos, D. A.; Pickett, W. E., Systematic Calculations of the Band Structures of the Rare-Gas Crystals Neon, Argon, Krypton, and Xenon. *Phys. Rev. B* **1988**, *38*, 6218.

33. Tsekouras, A. A.; Iedema, M. J.; Cowin, J. P., Amorphous Water-Ice Relaxations Measured with Soft-Landed Ions. *Phys. Rev. Lett.* **1998**, *80*, 5798-5801.

34. Ayotte, P.; Plessis, S.; Marchand, P., Trapping Proton Transfer Intermediates in the Disordered Hydrogen-Bonded Network of Cryogenic Hydrofluoric Acid Solutions. *Phys. Chem. Chem. Phys.* **2008**, *10*, 4785-4792.

35. Dubost, H., Infrared Absorption Spectra of Carbon Monoxide in Rare Gas Matrices. *Chem. Phys.* **1976**, *12*, 139-151.

36. Hagen, W.; Tielens, A. G. G. M., Infrared Spectrum of H_2O Matrix Isolated in CO at 10 K: Evidence for Bifurcated Dimers. *J. Chem. Phys.* **1981**, *75*, 4198-4207.

37. Ewing, G. E.; Pimentel, G. C., Infrared Spectrum of Solid Carbon Monoxide. *J. Chem. Phys.* **1961**, *35*, 925-930.

38. Bublitz, G. U.; Boxer, S. G., Stark Spectroscopy: Applications in Chemistry, Biology, and Materials Science. *Annu. Rev. Phys. Chem.* **1997**, *48*, 213-242.

39. Gibson, A. A. V.; Scott, T. A.; Fukushima, E., Anisotropy of the Chemical Shift Tensor for Solid Carbon Monoxide. *J. Magn. Reson.* **1977**, *27*, 29-33.

40. Li, F.; Brookeman, J. R.; Rigamonti, A.; Scott, T. A., ^{17}O NMR–NQR Study of Molecular Motion in the Liquid, and α and β Solid Phases of CO. *J. Chem. Phys.* **1981**, *74*, 3120-3130.

41. Shin, S.; Kang, H.; Cho, D.; Lee, J. Y.; Kang, H., Effect of Electric Field on Condensed-Phase Molecular Systems. II. Stark Effect on the Hydroxyl Stretch Vibration of Ice. *J. Phys. Chem. C* **2015**, *119*, 15596-15603.

42. Firanescu, G.; Signorell, R., Predicting the Influence of Shape, Size, and Internal Structure of CO Aerosol Particles on Their Infrared Spectra. *J. Phys. Chem. B* **2009**, *113*, 6366-6377.

43. Chang, H. C.; Richardson, H. H.; Ewing, G. E., Epitaxial Growth of CO on NaCl (100) Studied by Infrared Spectroscopy. *J. Chem. Phys.* **1988**, *89*, 7561-7568.

Figure for Table of Contents

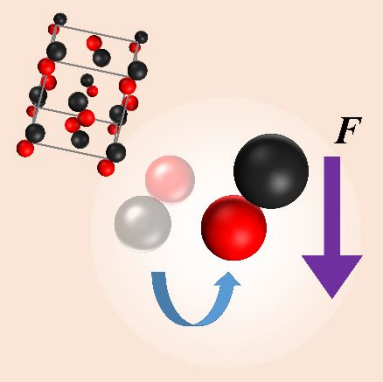

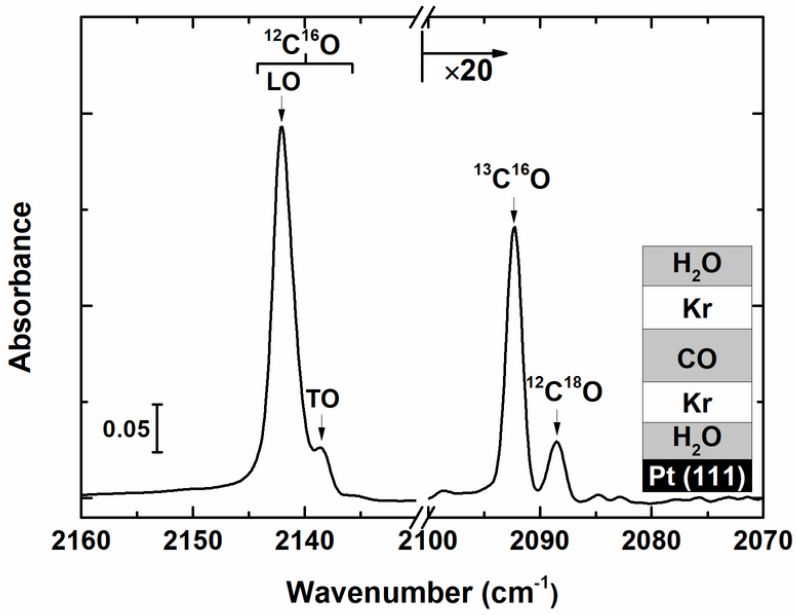

Figure 1

82x57mm (300 x 300 DPI)

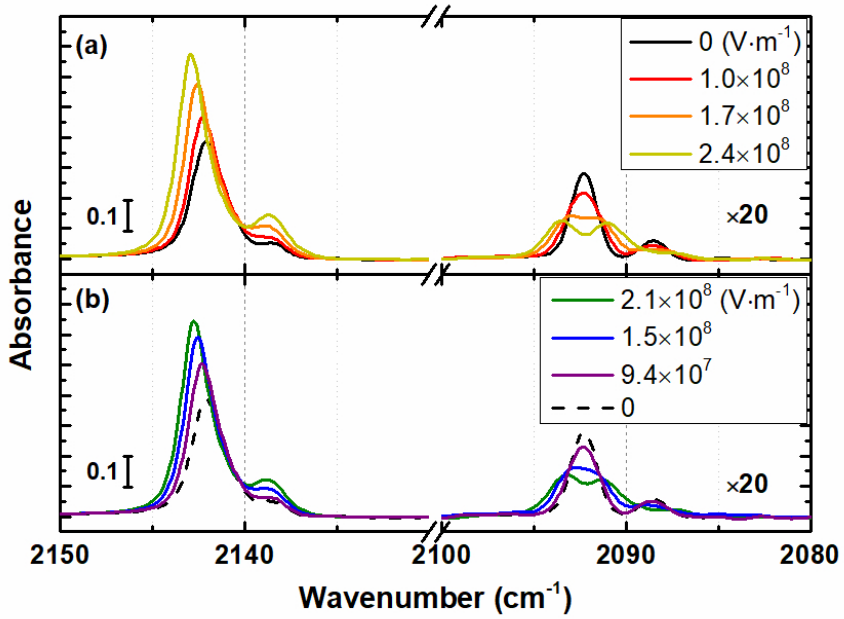

Figure 2

82x57mm (300 x 300 DPI)

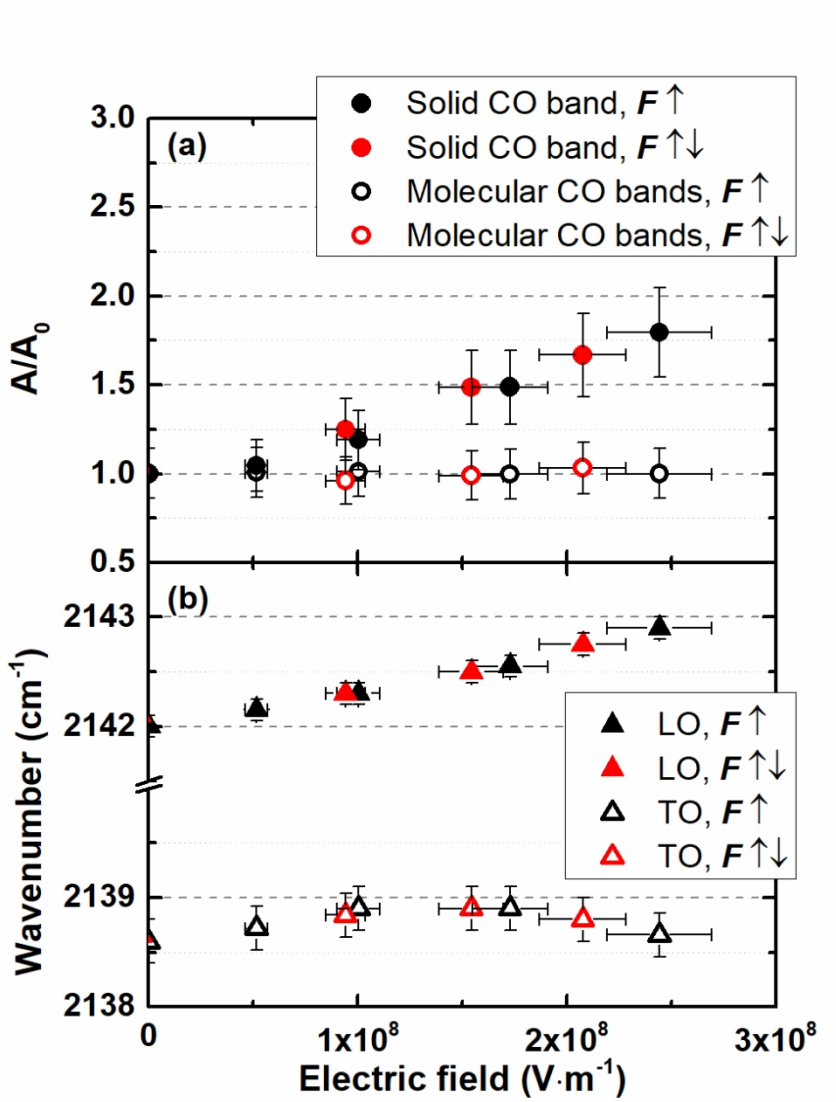

Figure 3

82x118mm (300 x 300 DPI)

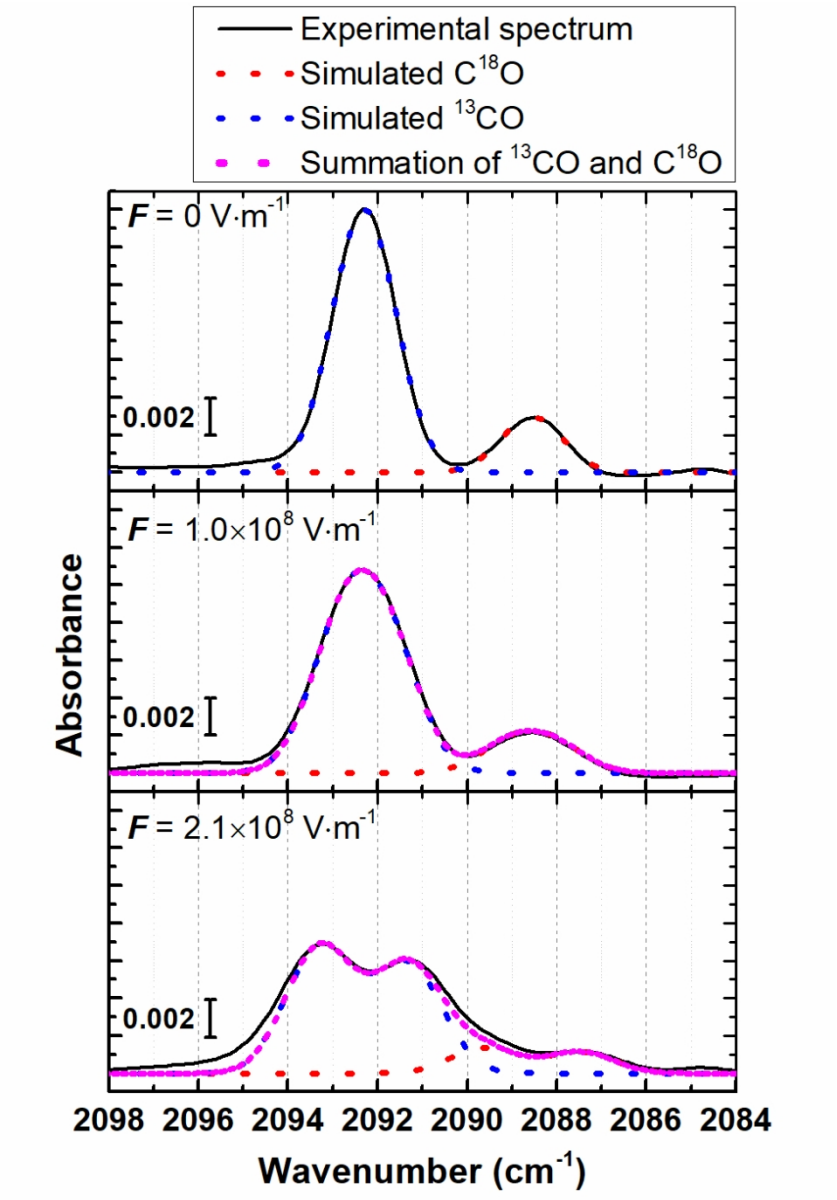

Figure 4

82x118mm (300 x 300 DPI)

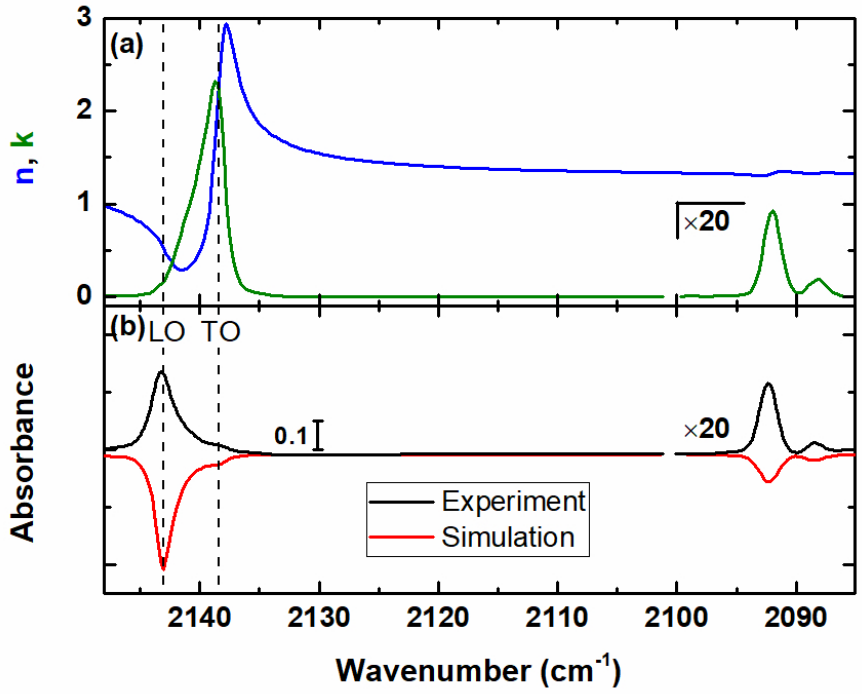

Figure 5

82x63mm (300 x 300 DPI)

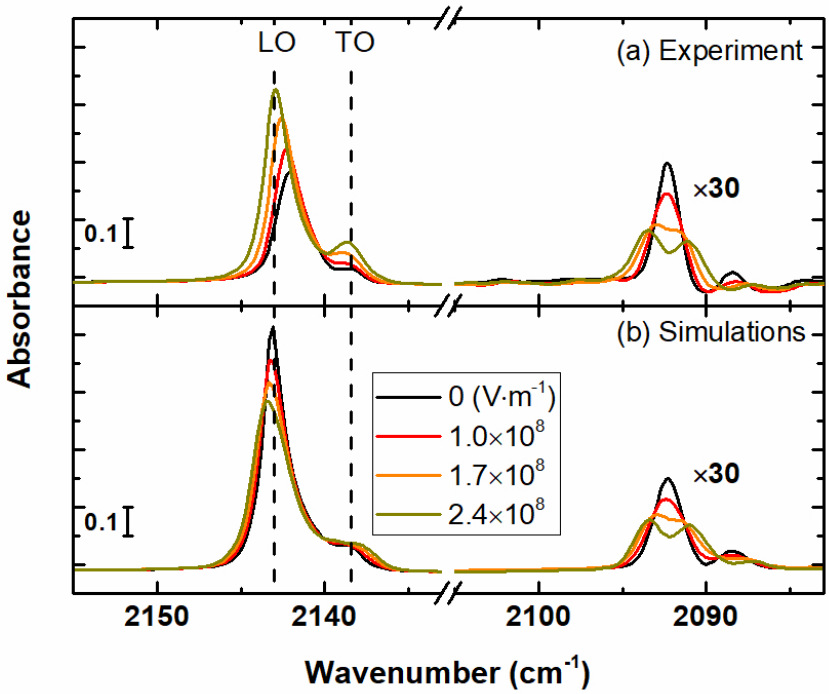

Figure 6

82x63mm (300 x 300 DPI)

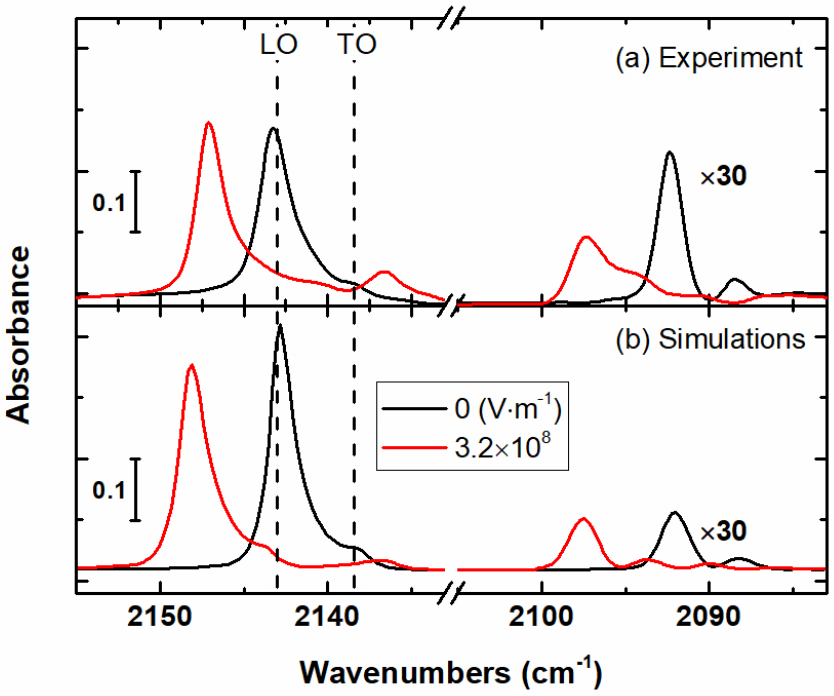

Figure 7

82x63mm (300 x 300 DPI)

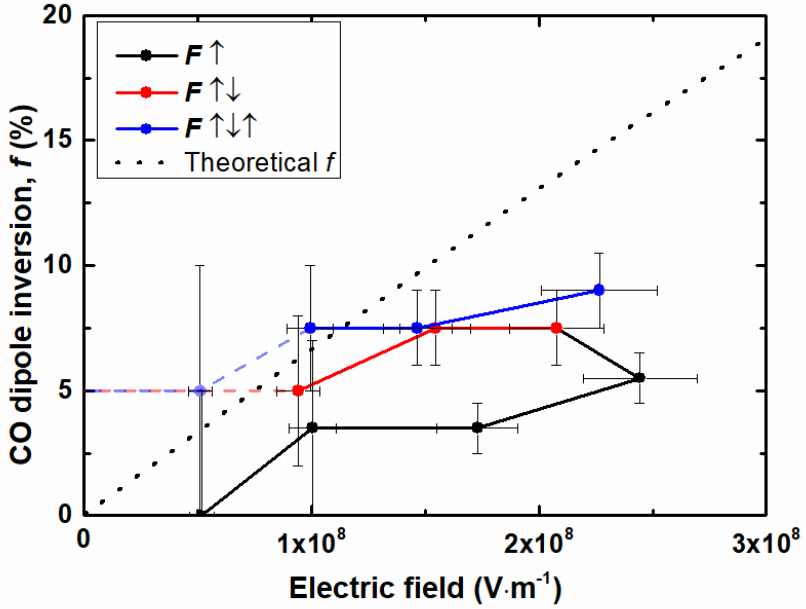

Figure 8

82x57mm (300 x 300 DPI)

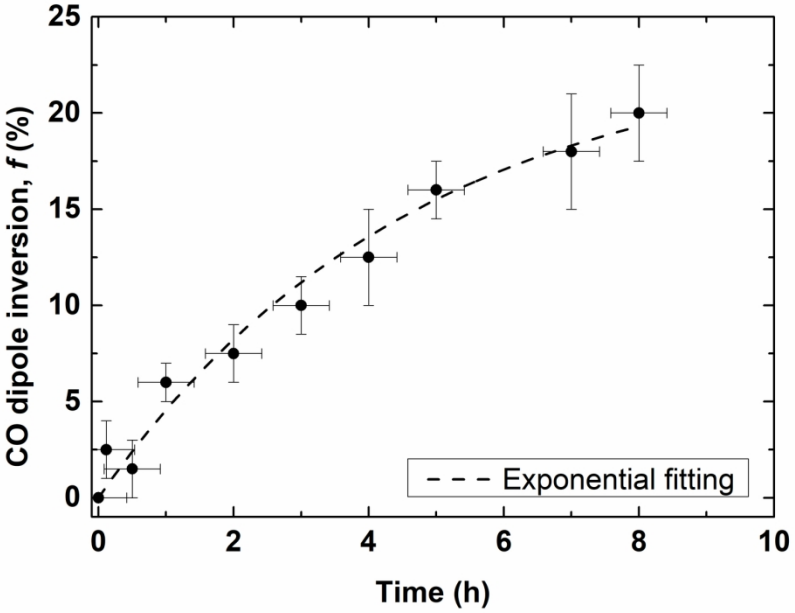

Figure 9

82x57mm (600 x 600 DPI)

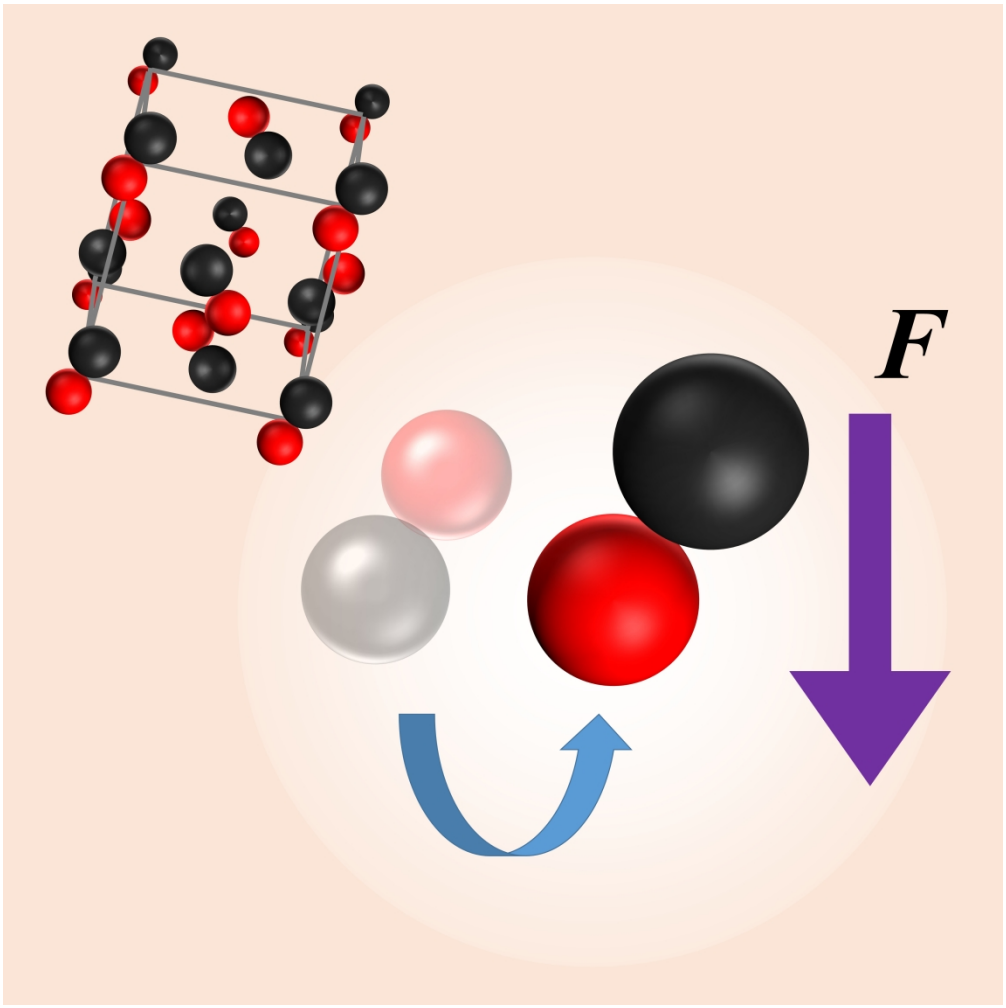

TOC Figure

329x329mm (300 x 300 DPI)